Journal of Power Sources 629 (2025) 235963

Contents lists available at ScienceDirect

Journal of Power Sources

journal homepage: www.elsevier.com/locate/jpowsour

Rapid Joule-heating synthesis of oxide nanoparticles on carbon cloth as electrodes for supercapacitors

Gang Chen [a,b,*], Maotang Wang [a], Mingzhi Jiao [a], Xianglin Kong [a], Lei Zhao [a,**]

[a] School of Information and Control Engineering, China University of Mining and Technology, Xuzhou, China
[b] School of Chemical Engineering and Technology, China University of Mining and Technology, Xuzhou, China

HIGHLIGHTS

- A Joule-heating strategy for the rapid incorporation of pseudocapacitive materials.
- The oxide nanoparticles are fabricated on preliminary activated carbon cloth.
- The advanced electrode based on Co_3O_4 exhibits high electrochemical performances.
- This method can be extended to various CC-based materials for supercapacitors.

GRAPHICAL ABSTRACT

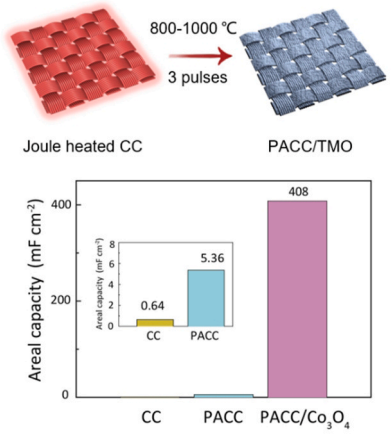

ARTICLE INFO

Keywords:
Joule-heating
Carbon cloth
Oxides nanoparticles
Supercapacitor electrodes

ABSTRACT

The rapid and controllable incorporation of pseudocapacitive materials onto the carbon cloth (CC) holds great promise for wearable supercapacitor devices. However, efficiently activating CC and achieving a high mass loading of electroactive materials remain challenging with conventional synthetic methods, which involve complex treatment and prolonged heating. This work presents a universal two-step strategy for the rapid preliminary activation of CC (PACC) and synthesis of composites using ultrafast high-temperature thermal shock (HTS) for CC/oxides-based electrodes. Pre-treated CC loaded with precursor materials is exposed to temperatures that rise swiftly to 1000 °C within 200 ms. Three electrical pulses, each lasting 100 ms, are applied and the entire process takes approximately 10 s. As a proof-of-concept, we synthesize a PACC/Co_3O_4 electrode material, which delivers a high specific capacity of 408 mF cm^{-2} at 0.2 mA cm^{-2}, 97 % capacity retention at 2 mA cm^{-2}, and excellent stability after 20,000 cycles. The flexible supercapacitor based on PACC/Co_3O_4 electrodes deliveres a high capacity and stable performance at various bending states. Moreover, our HTS method can be extended to

* Corresponding author. School of Information and Control Engineering, China University of Mining and Technology, Xuzhou, China.
** Corresponding author.
E-mail addresses: gangchen@cumt.edu.cn (G. Chen), leizhao@cumt.edu.cn (L. Zhao).

https://doi.org/10.1016/j.jpowsour.2024.235963
Received 6 September 2024; Received in revised form 22 November 2024; Accepted 26 November 2024
Available online 5 December 2024

other transition metal oxide (TMO) incorporated with the activated CC. The facile and efficient method paves the way for the synthesis of various CC-based supercapacitor materials.

1. Introduction

The pressing need to combat accelerated climate change and the ongoing depletion of fossil fuels has driven the development of high-efficiency energy storage system [1,2]. Among the state-of-the-art devices, supercapacitors stand out as promising candidates due to their higher power output, shorter charging time, and superior durability compared to other technologies under similar conditions [3]. To address key challenges, such as achieving high energy density, long cycling life, fast charge-discharge rate, and flexibility/deformability, various electrode materials have been developed.

The introduction of carbon fabric materials, such as the activated carbon cloth (ACC), has advanced the development of textile-powered portable electronic devices [4,5]. Compared to other candidates, ACC electrodes are expected to exhibit high conductivity, enhanced specific capacity, robust stability, and strong mechanical flexibility [6]. Currently, the activation of CC is primarily achieved through wet-chemistry methods (chemical oxidation/reduction and electrochemical oxidation) [7,8] or other physical/chemical techniques (gas-assisted annealing and plasma modification) [9,10], which result in complex processes and high energy consumption. Additionally, concerns regarding environmental and health impacts have been raised. To address these challenges, a Joule-heating method has been proposed in recent years for the rapid activation of CC [11,12]. Although the resulting ACC electrodes demonstrate excellent performance due to the dominant electric double-layer mechanism, the achieved specific capacitance remains limited and fails to meet the increasing demands for various applications. To further enhance energy storage performance, 1D CC fibers adorned with pseudocapacitive materials (e.g., transition metal compounds, TMCs) have been explored [13,14]. However, these capacitive guests are typically prepared in conventional furnaces, where the slow heating/cooling rates and prolonged reaction time (usually hours or even days at relatively low temperatures) cannot provide the harsh conditions needed to optimize the structure of the grown TMCs, often leading to aggregation [15–17]. Therefore, it is crucial to develop an effective strategy for fabricating ACC-based materials with high performances.

In this work, we present a novel approach for developing advanced supercapacitor electrodes, which involves rapid Joule heating of CC and the synthesis of transition metal oxides (TMOs) through an ultrafast high-temperature thermal shock (HTS) process. Unlike the previously mentioned methods (activation of CC and active material loading), our approach directly applies electric Joule heating to pre-treated CC for preliminary activation, enabling the formation of new TMOs on the CC (denoted as PACC/TMOs) to enhance energy storage capacity (Fig. 1). In a typical synthesis of these PACC/TMOs electrodes, commercial CC is first treated with a mixed acid solution, followed by HTS for rapid preliminary activation. In this step, HTS creates high temperatures around 800 °C with three durations of 100 ms. Note the transient heating presents difficulties in achieving the fully activated CC since carbon fibers cannot react sufficiently with oxygen, carbon dioxide and/or water in the air. For example, Guo's group activated CC through Joule-heating pyrolysis and the optimal reaction time reached 12.5 min [11]. Crucially, in the second step, HTS generates temperatures as high as 1000 °C within a short timescale (~200 ms), with the process lasting only 100 ms. The salt precursors decompose, nucleate, and grow into TMO nanoparticles (NPs) under elevated temperatures, as schematically illustrated in Fig. 1. The successive two-step HTS processes (three electrical pulses in each step) feature superior operational simplicity for CC/oxides synthesis, offering a facile, safe, and environment-friendly strategy for enhanced electrochemical performances of CC. To demonstrate the effectiveness of the Joule-heating method, we synthesized Co_3O_4 NPs on PACC as the electrode for a supercapacitor, which exhibited excellent electrochemical performance with an areal specific capacity of 408 mF cm^{-2} at 0.2 mA cm^{-2}, 97 % capacity retention at 2 mA cm^{-2}, remarkable stability after 20,000 cycles, and outstanding flexibility. Overall, this process provides a feasible route and can be easily extended to other TMO composites with CC, offering distinct advantages for electrode applications: (1) the synthesis of pseudocapacitive materials on PACC is rapidly achieved and the low-cost CC can be directly used as free-standing electrodes; (2) the transient non-equilibrium synthesis of TMOs during HTS prevents their excessive

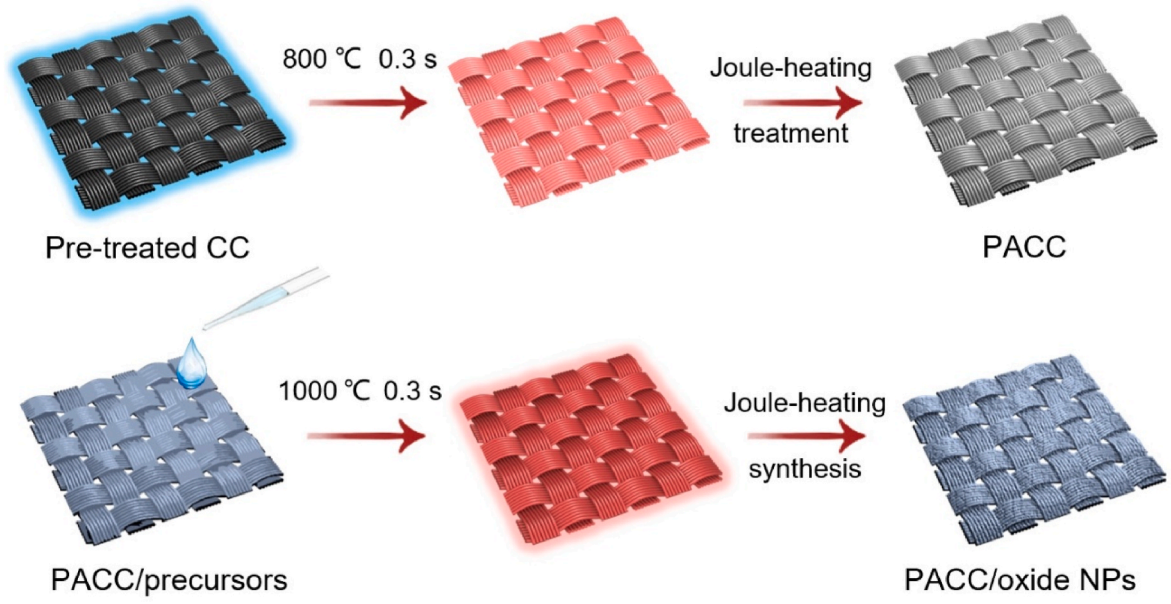

Fig. 1. Schematic illustration of both the preliminary activation of CC and the synthesis of oxide NPs via HTS.

growth and guarantees the close contact with PACC fibers, offering amplified mechanical stability and enhanced cycle performances; (3) the TMOs-incorporated PACC enabled by the energy-/time-saving HTS is promising for scalable production and may have broad potential for energy and catalysis applications.

2. Results and discussion

As a proof-of-concept, we first selected Co_3O_4 as a model material, known for its high theoretical specific capacity, to evaluate the effectiveness of our rapid synthesis approach for supercapacitor electrodes. The Joule-heating setup based on CC is illustrated in Fig. 2a. A CC heater was clamped between two crocodile clips connected to a programmable DC power supply, enabling rapid heating and ultrahigh temperatures. Various power levels were applied to maintain high temperatures (420–1242 °C) across CC samples of different sizes (from 1 to 5 cm in length). For instance, achieving a target temperature of 1000 °C requires larger electric power for longer CC pieces (Fig. 2b). The power input increases with the CC size and can be adjusted according to the specific application requirements. The temperature profile during the heating process of a 3 cm long CC was captured using an infrared thermometer (Fig. S1), as pictured in Fig. 2c. The PACC/Co_3O_4 NPs electrode was fabricated via a simple two-step HTS process: (1) preliminary activation of the pre-treated CC through direct Joule heating, and (2) synthesis of Co_3O_4 NPs by pulsing at ~1000 °C for 100 ms, repeated three times. Initially, a piece of CC sized 1 cm*3 cm was immersed in a solution containing strong oxidizing agents, including HNO_3 and H_2SO_4 for 48 h, followed by rapid treatment via Joule heating. Next, the HTS process for Co_3O_4 NPs was conducted, during which the high temperature completely decomposed the precursor with a Co^{2+} concentration of 1.25 mol/L (150 μL) loaded on the PACC, providing the atomic source for Co_3O_4 formation (see Methods for details) [10]. Notably, the performances of PACC/Co_3O_4 NPs were tested without any further modification or additional processing steps.

The morphology of the as-prepared sample was examined using a Scanning Electron Microscope (SEM). The surface of the PACC fibers was uniformly covered with Co_3O_4 NPs ranging in size from tens to hundreds of nanometers (Fig. 2d–e and S2a-c). While we increased the Co^{2+} loading (1.25 mol/L, 250 μL), the high loaded NPs with uniform spatial distribution were well preserved (Figs. S2d–f). According to the zoomed-in image (Fig. 2f) of Fig. 2e, it is observed that these NPs feature wrinkled surfaces, and a few are coated with smaller NPs approximately 0 nm in diameter. Additionally, the thermodynamics formation of PACC/Co_3O_4 can be easily tuned by varying the concentration of the metal salt precursor, enabling control over the nucleation and growth processes. Fig. 3g–i display the SEM images of PACC-based composites with different loadings of Co_3O_4 NPs. For example, at a small low Co^{2+} concentration of 0.25 mol/L, the carbon fibers were largely exposed, and negligible loading of NPs was observed (Fig. 2g). However, compared to the pristine CC (Fig. S3) and PACC (Fig. S4), the fiber surface became rough, with visible tracks and holes, as the $Co(NO_3)_2$ precursor decomposed into Co_3O_4 at elevated temperatures. This process functionalized the PACC, introducing multiscale defects, oxygen-containing functional groups as well as the Co_3O_4 NPs [8,10]. As we increased the Co^{2+} concentration to 0.50 and 0.75 mol/L, the rough fibers remained intact, and both the size and quantity of NPs grew. This morphology control can be attributed to the catalytic role of the numerous NPs in the carbon oxidation at high temperatures during HTS [10]. The stepwise formation mechanism of the Co_3O_4 on PACC fibers is thus hypothesized as follows: (1) the conductive PACC generates Joule heating to induce carbothermal shock, which ensures rapid decomposition of preloaded Co^{2+} precursors. (2) the in situ formed NPs (Co oxides and/or Co) at the

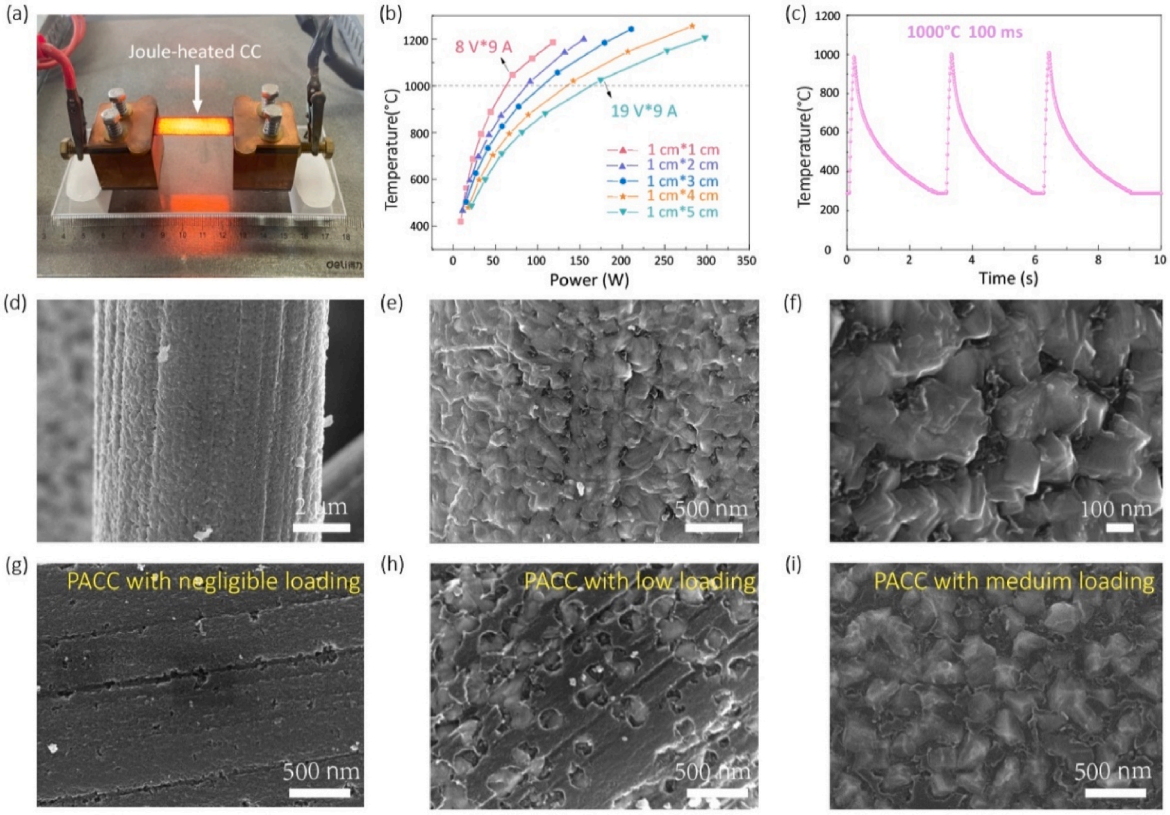

Fig. 2. Ultrafast Joule-heating synthesis of the PACC/Co_3O_4 electrode. (a) Digital images of the heated CC via electric Joule heating. (b) The temperature curves of bare CC with different sizes during Joule-heating. (c) The programed pulses for the synthesis of PACC/Co_3O_4 during HTS. (d–f) Morphology and structure of the PACC/Co_3O_4 composite at different magnifications. (g–i) Different loadings of the Co_3O_4 NPs on PACC fibers.

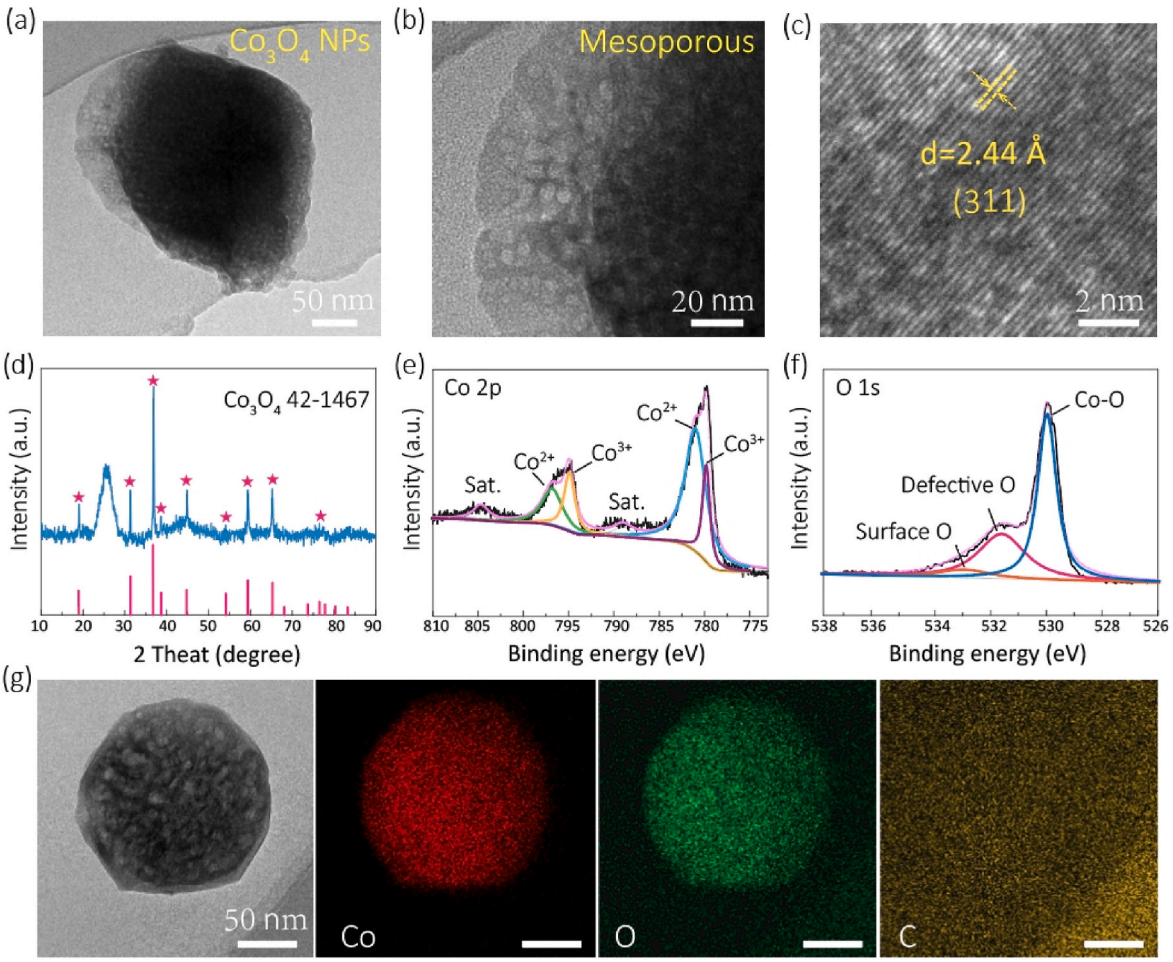

Fig. 3. Structural characterizations of the PACC/Co_3O_4 electrode. (a–b) TEM patterns of the Co_3O_4 NPs. (c) Atomic resolution HR-TEM image of the Co_3O_4 with highlighted (311) plane. (d) XRD pattern of the PACC/Co_3O_4 composite. (e–f) XPS spectra of Co 2p and O 1s, respectively. (g) HR-TEM image and EDS elemental maps of an individual mesoporous Co_3O_4 NP.

beginning promote the catalytic etch of carbon in the outer surface layer of PACC and move ultrafast. (3) the oxygen species (around NPs and in air) participate in a carbon oxidation reaction to functionalize PACC. (4) the ultrasmall Co_3O_4 NPs are finally synthesized via a transient non-equilibrium route during which the graphitization of modified PACC may also occur.

To further investigate the structure of PACC/Co_3O_4, we characterized the Co_3O_4 NPs using Transmission Electron Microscopy (TEM) technique. As shown in Fig. 3a–b and S5, the Co_3O_4 NPs with a size of approximately 150–200 nm exhibit a mesoporous structure with ultrathin edges, which enhances the electrochemical utilization of their surface. Fig. S6 shows the isotherms of PACC/Co_3O_4, which has a surface area of 3.9 $m^2\ g^{-1}$ as calculated by the Brunauer-Emmett-Teller (BET) method in the N_2 adsorption-desorption test. The value is slightly higher than that of pristine commercial CC (<1 $m^2\ g^{-1}$) due to the ultrathin Co_3O_4 layer and its horizontal spatial distribution on the surface of the CC fibers. Additionally, the formation of mesopores is confirmed by the Barrett-Joyner-Halenda (BJH) data (inset of Fig. S6), which exhibits a peak at 3.8 nm with an average pore size of 8.5 nm. The lattice fringes with an interplanar distance of 2.44 Å can be observed in the High-Resolution TEM (HR-TEM) image (Fig. 3c), corresponding to the (311) crystal plane of Co_3O_4 [18]. Fig. 3d shows an X-ray diffraction (XRD) pattern of the PACC/Co_3O_4 composite, which matches well with the standard Co_3O_4 pattern (#42–1467) [19]. The chemical states and composition of PACC/Co_3O_4 were further confirmed through X-ray photoelectron spectroscopy (XPS). The full spectrum in Fig. S7 indicates the main presence of Co, O, and C elements. The Co 2p peaks are divided into two groups (Co^{2+} and Co^{3+} species) alongside two weak satellite peaks [18]. After deconvolution, the typical peaks at 796.80 eV and 798.98 eV (Co $2p_{1/2}$) correspond to Co^{2+}, while those at 794.90 eV and 779.80 eV (Co $2p_{3/2}$) are attributed to Co^{3+}, confirming the co-existence of both Co^{2+} and Co^{3+} species (Fig. 3e) [18,20]. In the O 1s spectrum of PACC/Co_3O_4 (Fig. 3f), the binding energy at 529.97 eV belongs to the metal-oxygen band of Co-O. Additionally, the binding energies at 531.60 eV and 532.95 eV correspond to defective O and surface-adsorbed O, respectively [20]. Elemental mapping of an individual Co_3O_4 NP at high magnification shows a uniform distribution of Co and O across both particle and atomic scales (Fig. 3g).

To evaluate the electrochemical properties of PACC/Co_3O_4 synthesized via a two-step Joule-heating process, a three-electrode cell configuration was employed with 1 M KOH aqueous solution as the electrolyte. Fig. 4a presents the cyclic voltammetry (CV) curves of the PACC/Co_3O_4 electrode within a voltage window of 0–0.6 V at different scan rates ranging from 5 to 100 mV s^{-1}. The characteristic peaks in the CV curves indicate the existence of reversible Faradaic reactions, confirming the battery-type electrode behavior [21]. As the scan rate increases, the CV curve shapes remain largely unchanged, which reveals good electrochemical reversibility. The nonlinear nature of galvanic charge-discharge (GCD) curves at various current densities (Fig. 4b) further confirms the Faradaic pseudocapacitive characteristics [22]. Based on the discharge time at a current density of 0.2 mA cm^{-2}, the areal specific capacity is calculated to be approximately 408 mF cm^{-2}. The relationship between the specific capacity and the current density for PACC/Co_3O_4 is shown in Fig. 4c. And the corresponding gravimetric

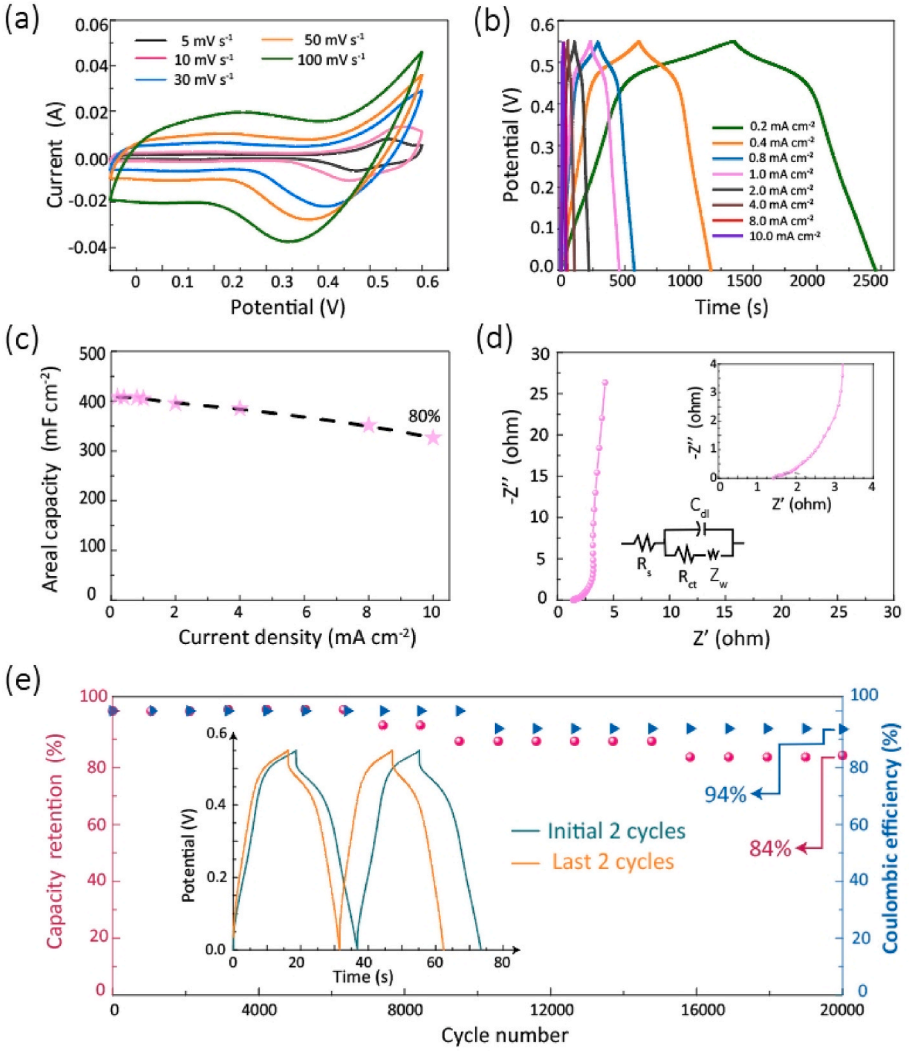

Fig. 4. Electrochemical properties of the PACC/Co_3O_4 electrode. (a) CV curves at different scan rates. (b) GCD curves at different current densities. (c) The relationship between areal capacity and current density. (d) Nyquist plot with the equivalent circuit model. (e) Long-term cycling performance at 10 mA cm^{-2} with an inset showing the initial and last two cycles.

specific capacities at current densities of 0.07, 0.14, 0.28, 0.35, and 0.7 A g^{-1} are 116.7, 116.5, 116.4, 115.9, and 113.1 F g^{-1}, respectively. It is found that the areal specific capacity remains at ~326 mF cm^{-2} (as high as 80 %) even when the current density increases from 0.2 to 10 mA cm^{-2}, implying good rate capability. In comparison, the capacitive performance of the pristine CC and PACC/Co_3O_4 is also assessed by the CV and GCD curves in Fig. S8 and the performance bar diagram in Fig. S9. The PACC/Co_3O_4 material via HTS endows the PACC a remarkably enhanced capacity from 5.36 mF cm^{-2} to ~408 mF cm^{-2}, which can be attributed to the added oxides as pseudocapacitive material. It is also worth mentioning that the capacity of the PACC/Co_3O_4 is comparable or even superior to those of other similar electrodes as reported [23–26].

To better evaluate the electrons and electrolyte ions transport through the PACC/Co_3O_4 electrode, an electrochemical impedance spectroscopy (EIS) study was performed. Fig. 4d presents the Nyquist plot and the corresponding equivalent circuit diagram. The series resistance (R_s) in the equivalent circuit represents the solution resistance of the system, while faradaic charge-transfer resistance (R_{ct}) refers to the characteristics of the contact between the electrode and the electrolyte at high-medium frequencies, represented by the diameter of the semicircle [27]. The results after fit with the software of Z-view reveal that the R_s and R_{ct} values of PACC/Co_3O_4 electrode are 1.45 Ω and 1.15 Ω, respectively. Accordingly, the low values of both R_s and R_{ct} could arise from the close contact between the active Co_3O_4 NPs and conductive PACC skeleton. To further investigate the cyclic stability of the PACC/Co_3O_4 electrode, successive GCDs were carried out at a current density of 10 mA cm^{-2} (Fig. 4e). After 20,000 cycles, the specific capacity retained 84 % of its initial value (326 mF cm^{-2}), amounting to 274 mF cm^{-2}. The inset shows the first and last two cycles, indicating a consistent and stable cycling behavior. Additionally, the Coulombic efficiency remained ~94 % throughout the whole entire charge/discharge cycles, revealing the high charge transfer efficiency. The above results suggest that the PACC/Co_3O_4 composite synthesized via HTS is a promising material for high-performance supercapacitor electrodes.

To demonstrate its potential for practical application, the PACC/Co_3O_4 electrode was assembled into an all-solid-state supercapacitor (ASSSC), as shown in Fig. S10a. CV and GCD curves were used to characterize its electrochemical performance. The CV curves in Fig. S10b demonstrated obvious oxidation/reduction peaks and all the curve shapes remained unchanged, implying the good rate performance. According to the GCD curves in Fig. S10c, a maximum areal capacity of 48.7 mF cm^{-2} was obtained at 0.2 mA cm^{-2} for ASSSC and ~89 % areal capacity (43.1 mF cm^{-2}) was achieved as the current density reached 4 mA cm^{-2} (Fig. S10d). Moreover, the bending performance was studied and the ASSSC was found to be still functional under severe mechanical

deformation conditions between the bending angles of 45°–180°, as displayed in Fig. S11. The CV curves at a scan rate of 30 mV s^{-1} showed only subtle changes even at various bending angles. Besides, based on the discharge time at a current density of 0.2 mA cm^{-2} in GCD curves, the areal capacities were calculated to be in a narrow range from 44.5 to 46.8 mF cm^{-2}, indicating the excellent flexibility of ASSSC without degraded performance.

In addition to the Co_3O_4 electrode, our approach can be easily extended to other oxide materials by utilizing different metal salt precursors. As another demonstration, we successfully synthesized the PACC/MnO_x electrode (inset of Fig. 5a and Fig. S12) using the two-step HTS. The XRD pattern (Fig. 5a) reveals the diffraction peaks corresponding to Mn_2O_3 (#41–1442) and Mn_3O_4 (#24–0734), despite the strong peaks from the carbon substrate, indicating the co-existence of two manganese oxide phases. The electrochemical studies on PACC/MnO_x electrode were also conducted by adopting a three-electrode system. Fig. S13 presents the CV curves of PACC/MnO_x at various scan rates. As the scan rate increases, no significant polarization is observed, demonstrating its high-rate capability [28].[22] The maximum areal specific capacity is calculated to be ~456 mF cm^{-2} according to the GCD curves in Fig. 5b. The corresponding gravimetric specific capacity is 130.3 F g^{-1} at a current density of 0.07 A g^{-1}. Furthermore, as the current density increases from 0.2 to 2.0 mA cm^{-2}, the specific capacity remains high at ~325 mF cm^{-2}, which is 71 % of the capacity at 0.2 mA cm^{-2}, as shown in Fig. 5c. Compared to conventional techniques, our Joule-heating HTS method offers several advantages [29–33], including (1) universality of carbon substrates with various TMO NPs with superior operation simplicity, (2) high synthesis temperatures (>1000 °C) with short heating duration (100 ms) for energy saving, (3) significantly time-saving synthesis (within 10 s), and (4) fast heating/quenching rates (ramping to 1000 °C in just 200 ms and cooling to 300 °C in <2 s).

3. Conclusion

In this study, we demonstrate the use of HTS technique for the rapid synthesis of PACC/Co_3O_4 composites as electrodes for supercapacitors. Through direct Joule heating during HTS, Co_3O_4 NPs are rapidly introduced at ~1000 °C with three 100 ms pulse durations, during which the salt precursors decompose quickly to form oxide NPs. The PACC/Co_3O_4 electrode exhibited an areal specific capacity of 408 mF cm^{-2} at 0.2 mA cm^{-2}, with 97 % capacity retention at 2 mA cm^{-2}, and demonstrated excellent durability after 20,000 cycles. Additionally, the assembled ASSSC device delivered a high capacity of 48.7 mF cm^{-2} at 0.2 mV s^{-1} and displayed stable performance at various bending states. As further proof-of-concept, MnO_x NPs were also synthesized on PACC fibers, achieving a high areal specific capacity of ~456 mF cm^{-2} at 0.2 mA cm^{-2}. The reported HTS method can be applied to various CC-based materials, thereby offering a facile, safe, and environment-friendly strategy for supercapacitor applications.

4. Methods

Materials. Plain CC (WOS1011) was obtained from CeTech Co. Ltd. Cobalt nitrate hexahydrate ($Co(NO_3)_2{\cdot}6H_2O$), manganese nitrate tetrahydrate ($Mn(NO_3)_2{\cdot}4H_2O$), and potassium hydroxide (KOH) were purchased from Aladdin. All materials were used as received without further treatment.

Preparation of PACC/TMO NPs composites. The commercial CC was first cut into small pieces (e.g., 1 cm* 3 cm). Before undergoing

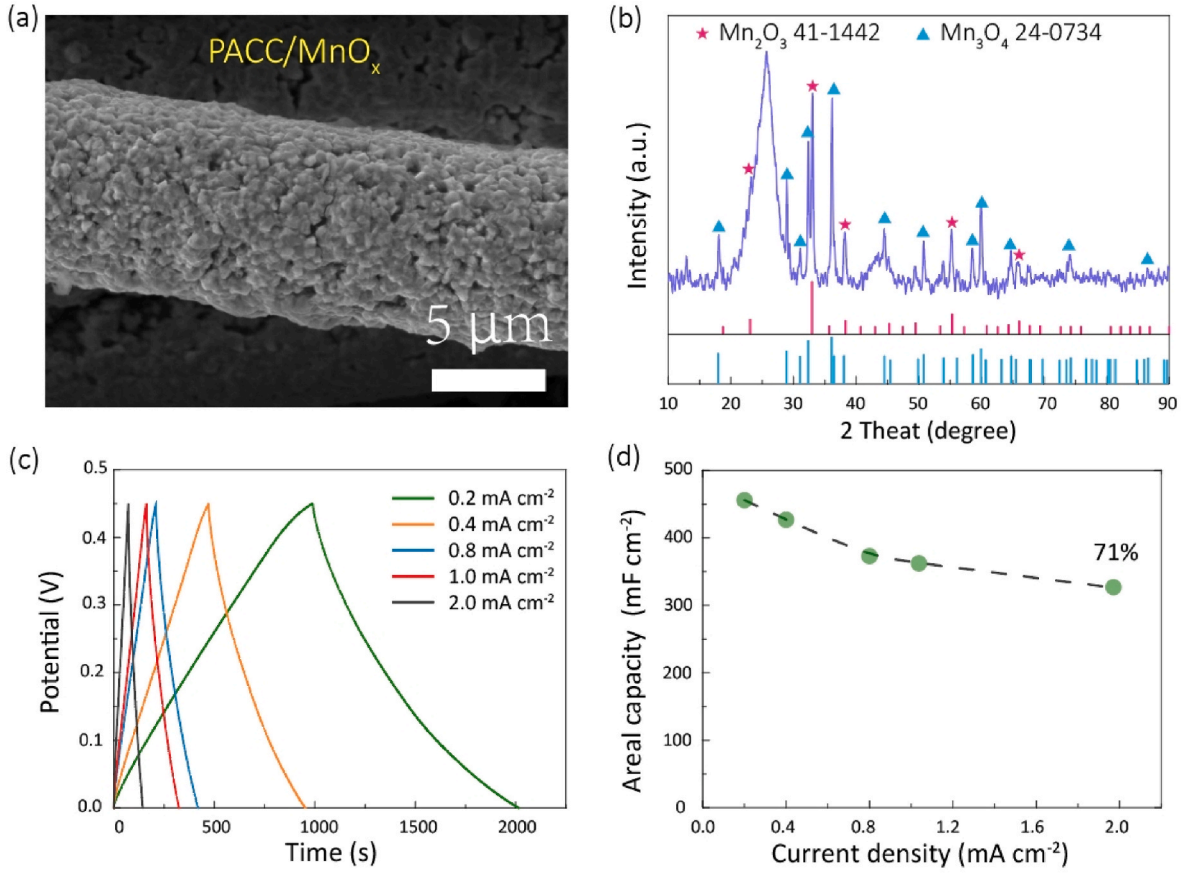

Fig. 5. Universality of the Joule-heating HTS method. (a) The morphology of MnO_x NPs on a PACC fiber. (b) XRD pattern of the PACC/MnO_x. (c) GCD curves of the PACC/MnO_x electrode at different current densities. (d) The relationship between the areal capacity of PACC/MnO_x and current density.

Joule-heating treatment, the CC was immersed in a mixed acid solution of HNO_3 and H_2SO_4 (1:1 volume-volume ratio) for 48 h. After the acid treatment, the pre-treated CC was thoroughly cleaned with ethanol and deionized water in an ultrasonic bath, followed by drying at 50 °C in air for 24 h. The pre-treated CC was then subjected to rapid thermal shock (100 ms at ~800 °C, three pulses) in an air-filled glovebox to obtain PACC. The precursor solution was then added dropwise onto the surface of the PACC (1.25 mol/L*150 μL), and HTS (100 ms at ~1000 °C, three pulses) was applied to convert PACC/precursor into the PACC/TMO composite. The heater temperature was monitored by an IR camera equipped in the HTS setup (ZKJY-HTS), with a measurement range from 300 to 1600 °C. Finally, the resulting product was thoroughly washed with deionized water and ethanol before drying.

Materials Characterization. Field-emission SEM (FE-SEM) characterization of the PACC/TMO composites was conducted using MAIA3 LMH system. The microstructure was examined by field-emission TEM equipped with EDS (FE-TEM, Tecnao G2 F20 operated at 200 kV). The specific surface area and pore size were analyzed using a Micromeritics ASAP-2460 (Micromeritics Instrument Corp.) by the adsorption/desorption of N_2. XRD test was performed to investigate the crystal structure using a D8 Advanced system with Cu Kα radiation. Elemental chemical compositions were determined by XPS on an ESCALab250Xi system with Al Kα radiation.

Electrochemical measurement. The electrochemical characterizations, including CV, GCD, EIS, and cycle testing, were conducted using an electrochemical workstation (Shanghai CHI 760E) in a three-electrode system. Pt foil was used as the counter electrode and a Hg/HgO electrode was employed as a reference electrode. The PACC/Co_3O_4 and PACC/MnO_x materials, both of which possess the oxides loading of ~3.5 mg cm^{-2}, served as the working electrodes (1 cm * 0.9 cm) in 1M KOH electrolyte. The areal specific capacity (C_s, mF cm^{-2}) of the electrode was calculated using the equations: $C_s = J_s\Delta t/\Delta V$, where J_s is the areal current density (mA cm^{-2}), Δt is the discharge time (s), and ΔV is the potential window (V). While the mass specific capacity (C_m, F g^{-1}) of the electrode was calculated from the following equations: $C_m = J_m\Delta t/\Delta V$, where J_m is the mass current density (A g^{-1}).

All-solid-state supercapacitor (ASSSC) assembly. ASSSCs were fabricated by employing PACC/Co_3O_4 as both the cathode and anode. The KOH/PVA gel, which acted as the solid electrolyte, was prepared by mixing 1.5 g of PVA, 1.0 g of KOH, and 18 mL of deionized water, followed by heating (around 95 °C) with continuous stirring until a transparent gel was obtained. After natural cooling, slow stirring (~2 h) was conducted to remove any trapped bubbles. The prepared gel was then casted onto one side of PACC/Co_3O_4 electrode. Finally, a piece of filter paper soaked with KOH/PVA gel was sandwiched between the two PACC/Co_3O_4 electrodes to fabricate an ASSSC device (PACC/Co_3O_4//PACC/Co_3O_4).

CRediT authorship contribution statement

Gang Chen: Writing – review & editing, Writing – original draft, Supervision, Investigation, Funding acquisition, Data curation. **Maotang Wang:** Methodology, Investigation, Formal analysis, Data curation. **Mingzhi Jiao:** Resources. **Xianglin Kong:** Project administration, Methodology. **Lei Zhao:** Writing – review & editing, Supervision, Resources, Project administration, Methodology, Investigation, Conceptualization.

Declaration of competing interest

No conflict of interest statement

Acknowledgements

The authors kindly acknowledge the support by the Fundamental Research Funds for the Central Universities (No. 2024QN11020). We also thank Dr. Yanwei Sui and Dr. Danyang Zhao, professors from China University of Mining and Technology, for assistance in the experiments of all-solid-state supercapacitors.

Appendix A. Supplementary data

Supplementary data to this article can be found online at https://doi.org/10.1016/j.jpowsour.2024.235963.

Data availability

Data will be made available on request.

References

[1] P.W. Xiao, Q. Meng, L. Zhao, J.J. Li, Z. Wei, B.-H. Han, Mater. Des. 129 (2017) 164–172.
[2] M. Qorbani, K.H. Chen, L.C. Chen, Small (2024) e2400558.
[3] C. Zhang, H. Du, K. Ma, Z. Yuan, Adv. Energy Mater. (2020) 10.
[4] Z. Yan, S. Luo, Q. Li, Z.S. Wu, S.F. Liu, Adv. Sci. 11 (2024) e2302172.
[5] A. Bhardwaj, U. Okoroanyanwu, J.N. Pagaduan, W. Fan, J.J. Watkins, Small (2024) e2402049.
[6] Y. Xu, S. Yu, H.M. Johnson, Y. Wu, X. Liu, B. Fang, Y. Zhang, iScience 27 (2024) 108786.
[7] G. Wang, H. Wang, X. Lu, Y. Ling, M. Yu, T. Zhai, Y. Tong, Y. Li, Adv. Mater. 26 (2014) 2676–2682, 2615.
[8] W. Wang, W. Liu, Y. Zeng, Y. Han, M. Yu, X. Lu, Y. Tong, Adv. Mater. 27 (2015) 3572–3578.
[9] Y.J. Gu, W. Wen, J.M. Wu, J. Mater. Chem. A 6 (2018) 21078–21086.
[10] G. Zhong, S. Xu, Q. Dong, X. Wang, L. Hu, Adv. Funct. Mater. 31 (2021).
[11] X. Sun, S. Hou, L. Yuan, F. Guo, Carbon Lett 32 (2022) 1745–1756.
[12] S. Li, Y. Zhao, P. Shi, J. Zhou, J. Long, N. Cao, J. Liu, F. Meng, Adv. Eng. Mater. (2023) 25.
[13] M.R. Abdul Karim, W. Shehzad, J. Energy Storage (2023) 72.
[14] K. Ren, Z. Liu, T. Wei, Z. Fan, Nano-Micro Lett. 13 (2021) 129.
[15] J. Li, L. Luo, S. Wang, H. Song, B. Jiang, PhotoMat (2024).
[16] W. Shi, Z. Li, Z. Gong, Z. Liang, H. Liu, Y.-C. Han, H. Niu, B. Song, X. Chi, J. Zhou, H. Wang, B.Y. Xia, Y. Yao, Z.-Q. Tian, Nat. Commun. (2023) 14.
[17] T. Tsuzuki, Commun. Chem. 4 (2021) 143.
[18] L. Zhang, T. Zhang, K. Dai, L. Zhao, Q. Wei, B. Zhang, X. Xiang, RSC Adv. 10 (2020) 29326–29335.
[19] J. Sun, H. Wang, Y. Li, M. Zhao, J. Porous Mater. 28 (2021) 889–894.
[20] W. Li, X. He, B. Li, B. Zhang, T. Liu, Y. Hu, J. Ma, Appl. Catal., B 305 (2022).
[21] W. Fan, F. Wang, X. Xiong, B. Song, T. Wang, X. Cheng, Z. Zhu, J. He, Y. Liu, Y. Wu, NPG Asia Mater. 16 (2024).
[22] Y. Sun, D. Jiang, J. Wang, A. Zhang, C. Wang, H. Zong, J. Xu, J. Liu, Small 20 (2024) e2305288.
[23] S.A. Pawar, D.S. Patil, D.K. Nandi, M. Monirul Islam, T. Sakurai, S.-H. Kim, J. Cheol Shin, J. Chem. Eng. 435 (2022).
[24] M. Khandelwal, A.P. Nguyen, C.V. Tran, J.B. In, RSC Adv. 11 (2021) 38547–38554.
[25] C. Guan, X. Qian, X. Wang, Y. Cao, Q. Zhang, A. Li, J. Wang, Nanotechnol. 26 (2015) 094001.
[26] F. Yang, K. Xu, J. Hu, J. Alloys Compd. 729 (2017) 1172–1176.
[27] X. Yang, Q. He, L. Hu, W. Wang, W. Chen, X. Fang, J. Liu, Molecules (2024) 29.
[28] S. Shao, S. Liu, C. Xue, Nanomaterials (2023) 13.
[29] X. Cui, Y. Liu, X. Wang, X. Tian, Y. Wang, G. Zhang, T. Liu, J. Ding, W. Hu, Y. Chen, ACS Nano 18 (2024) 2948–2957.
[30] X. Cui, W. Li, Y. Liu, Y. Zhu, Y. Chen, C. Gong, G. Xue, J. Mater. Sci. Tech. 191 (2024) 1–7.
[31] X. Cui, Y. Liu, Y. Chen, Natl. Sci. Rev. 11 (2024) nwae033.
[32] J. Huang, S. Zhu, J. Zhang, G. Han, ACS Mater. Lett. 6 (2024) 2144–2152.
[33] L. Zong, F. Lu, P. Li, K. Fan, T. Zhan, P. Liu, L. Jiang, D. Chen, R. Zhang, L. Wang, Adv. Mater. (2024) e2403525.